Combustion and Flame 270 (2024) 113759

Contents lists available at ScienceDirect

Combustion and Flame

journal homepage: www.sciencedirect.com/journal/combustion-and-flame

Direct numerical simulations of turbulent premixed cool flames: Global and local flame dynamics analysis

Yiqing Wang [a,1], Chao Xu [b], Cheng Chi [c], Zheng Chen [a,*]

[a] SKLTCS, HEDPS-CAPT, College of Engineering, Peking University, Beijing, 100871, China
[b] Transportation and Power Systems Division, Argonne National Laboratory, Lemont, 60439, IL, USA
[c] Lab. of Fluid Dynamics and Technical Flows, University of Magdeburg "Otto von Guericke", Germany

ARTICLE INFO

Keywords:
Cool flames
Turbulent premixed flames
Turbulent burning velocity
Flame displacement speed

ABSTRACT

The cool flame dynamics, especially in turbulent flows, is of great interest for both practical application and fundamental research. In this study, a series of direct numerical simulations of turbulent premixed *n*-$C_7H_{16}/O_2/O_3/N_2$ cool flames are performed, with the focus on the influence of turbulence intensity (u'/S_L, where S_L is the laminar flame speed) on the flame structure as well as the global and local cool flame dynamics. It is found that the cool flame front is considerably wrinkled by turbulence at high u'/S_L, leading to significantly thickened turbulent cool flame brush and largely altered local reactivity compared with the reference laminar flame. However, the turbulent flame structure in the temperature space is found to be insensitive to u'/S_L. Besides, with increasing u'/S_L, the normalized turbulent cool flame speed (S_T/S_L) is monotonically increased, attributed to substantial augmentation on the flame surface area (A_T/A_L), while the stretching factor (I_0) remains almost constant and is smaller than 1. The underlying mechanisms for such variations are revealed through local flame dynamics analysis. Specifically, the local flame displacement speed S_d is found to be strongly negatively correlated with flame curvature; meanwhile, such negative correlation and the probability distribution function (PDF) of flame curvature are barely influenced by u'/S_L, leading to a weak dependence of I_0 on u'/S_L. In contrast, the PDF of the tangential strain rate is found to span a much wider range and shift to the positive side as u'/S_L increases, suggesting that the enhanced tangential strain rate is the main cause for the increase in surface area of the turbulent premixed cool flame. Finally, the influence of equivalence ratio on above findings is found to be insignificant, indicating that although the local reactivity of turbulent premixed cool flames is altered due to the differential diffusion, the resultant flame-stretch interaction is insensitive to the equivalence ratio. This study presents some unique cool flame dynamics that are distinct from hot flames, which can help improve the understanding and modeling of turbulent cool flames.

Novelty and Significance Statement

The novelty of this work is that the combined global and local flame dynamics analyses are conducted for isolated turbulent premixed cool flames for the first time. It is found that with increasing turbulence intensity, the normalized turbulent cool flame speed increases monotonically due to substantial increase on flame surface area, whereas the stretching factor remains almost constant. The underlying mechanisms for these trends are revealed through the local flame dynamics analysis. Besides, the influence of equivalence ratio is found to be insignificant on the cool flame dynamics. Results from this work demonstrate that the turbulent premixed cool flame features some similar characteristics as the turbulent hot flames with Lewis number larger than 1, but more importantly, it also present some unique characteristics which are distinct from hot flames. Therefore, this study contributes to a better understanding of cool flame dynamics.

* Corresponding author.
E-mail address: cz@pku.edu.cn (Z. Chen).
[1] The authour is currently at Argonne National Laboratory.

https://doi.org/10.1016/j.combustflame.2024.113759
Received 20 June 2024; Received in revised form 20 September 2024; Accepted 26 September 2024
Available online 4 October 2024

1. Introduction

The cool flame, which is governed by low-temperature chemistry (LTC) [1], has received renewed interest in the last two decades due to its large impacts on the combustion process in many high-efficiency, low-emission engines [1,2]. For example, the previous studies [2–4] have demonstrated that under engine-relevant conditions, the LTC ignition kernel is usually first initiated and then transitions to a transport-supported cool flame propagating toward rich mixtures, which substantially influences the timing and location of the subsequent high temperature ignition. Therefore, the cool flame dynamics, especially under turbulence conditions, is of great interest for both practical application and fundamental research.

Extensive experimental and numerical studies have been conducted for laminar cool flames to better understand the structure and dynamics of cool flames [1]. In particular, based on the counterflow configuration, the stabilized and isolated premixed and non-premixed cool flames have been experimentally established [5,6], enabling direct measurement of cool flame ignition and extinction limits. By using a Hencken burner with ozone addition, Belmont and coworkers [7,8] established the freely propagating cool flames and measured the isolated laminar cool flame speeds which is a critical cool flame property. Through 1D simulations with detailed chemistry, Yang and Zhao [9] investigated the stretch effect on premixed cool flame dynamics and found that the stretched cool flame speed is always negatively correlated with stretch rate regardless of the equivalence ratio, a feature that is distinct from hot flames. Such phenomenon was also observed in the 2D simulations conducted by Wang et al. [10] where the cool flame propagates in a mixing layer. The response of cool flame propagation speed in stratified mixtures is also found to be different from that of hot flames [11]. These laminar flame studies have revealed the unique characteristics of cool flame dynamics which are associated with LTC.

Some recent efforts have been devoted to the turbulence-LTC interactions and turbulent cool flames at engine-relevant conditions [3,4,12]. However, these studies have mainly focused on the impacts of LTC and cool flames on the multi-stage and multi-mode ignition process, while there are only few studies on isolated turbulent cool flames [13–16]. Novoselov et al. [14] conducted a combined experimental and numerical investigation for turbulent non-premixed cool flames, and reported the unity effective Lewis number transport of turbulent non-premixed cool flames. Savard et al. [16] numerically studied turbulent premixed cool flames and found that a LTC supported ignition front was able to transition to a self-propagating cool flame due to turbulent diffusion. These turbulent premixed cool flames were found to be strongly distributed, whereas the reaction zone structure and global chemical pathways remain similar to the reference laminar cool flame. Besides, they reported that the burning efficiency factor (or stretch factor I_0) was larger than 1 for turbulent premixed cool flames [16], which is, to some extent, contradictory to the negative correlation between flame speed and stretch rate observed in laminar premixed cool flames [9]. In this context, the dynamics of premixed cool flames has not been well understood. Moreover, to the authors' best knowledge, the flame-stretch interaction in turbulence environment as well as its influence on the global propagation speed of turbulent premixed cool flame has not been studied.

Therefore, the objective of this study is to investigate the isolated turbulent premixed cool flames, with the focus on the analysis for both global and local flame dynamics. A series of direct numerical simulations (DNS) are conducted for turbulent premixed n-$C_7H_{16}/O_2/O_3/N_2$ cool flames subjected to different turbulence intensities. Besides, considering that the flame-stretch interaction is very sensitive to equivalence ratio for hot flames, the influence of equivalence ratio on turbulent premixed cool flames is also investigated. The same mixture and thermodynamic conditions as in the experiments measuring laminar cool flame speeds [7,8] are considered in this study.

2. Numerical methods and flame configurations

2.1. Numerical configuration

As shown in Fig. 1, the statistically-planar turbulent premixed flame configuration adopted in [15,16] is considered. Specifically, a turbulent premixed n-C_7H_{16} cool flame propagates along the streamwise direction (y) in a box with the size of $L_x \times L_y \times L_z$ where L_y=6L and $L_x = L_z = L$. The inflow and outflow conditions are imposed in the streamwise y direction, with periodic boundary conditions in lateral x- and z-directions. A non-reacting, statistically stationary homogeneous isotropic turbulence (HIT) is first computed to initialize the flow field and is also imposed to the bulk inlet flow. Then a laminar premixed cool flame computed from Cantera [17] is mapped along the y-direction with the flame front located at the center of domain. To maintain the turbulence with prescribed intensity, a linear velocity forcing method [18] is applied to generate turbulence in the region from y=0.5L to 5L. This method has been used in many previous DNS studies with the same configuration [16,19,20], and has been demonstrated to leave the small-scale behavior essentially unaltered [18]. Besides, in [20], the turbulent flame dynamics in forced and decaying HIT were studied, and very similar turbulence-flame interactions were observed. In the present DNS, the mean inlet velocity is adjusted based on the active-control algorithm of Bell et al. [21] to statistically anchor the turbulent flame brush at the center of domain. All the analysis is conducted for the flame that has reached a statistically steady state.

The low Mach number Navier–Stokes equations are solved using the finite difference DNS solver DINO [22]. A sixth-order finite-difference method is used for spatial discretization and a semi-implicit third-order Runge–Kutta method is employed for temporal integration. The mixture-averaged transport model is adopted to calculate molecular diffusion fluxes. The chemical reaction rates as well as the thermal and transport properties are computed by Cantera [17].

2.2. Flame properties and turbulence parameters

As mentioned before, Belmont and co-workers [7,8] measured the laminar cool flame speed for n-$C_7H_{16}/O_2/O_3/N_2$ mixtures, which has been the very rare experimental data for cool flame speed up to date. They also provided a reduced mechanism which is a subset of the Lapointe mechanism [23] appended with O_3 sub mechanism [24]. This reduced mechanism has restricted the kinetic pathway transition from cool flame chemistry to hot flame chemistry to achieve an isolated cool flame without the trailing hot flame, and was demonstrated to have a good accuracy in predicting the cool flame speed as well as flame structure (such as flame temperature and formaldehyde intensity) for n-C_7H_{16}. Therefore, in this DNS study, we adopted the same mixture composition, thermodynamic conditions, and reduced mechanism (41 species and 196 reactions) used in [7,8] to ensure that the simulated cool flames are realistic, and the chemical mechanism used has been validated against cool flame data. The initial O_2/N_2 volume ratio is 3.81:1 and then a small amount of O_2 is replaced by O_3, leading to 5.5% O_3 concentration in O_2/O_3 by volume. The temperature and the pressure are fixed at T_u=392 K and P = 22.7 kPa as in [8]. To the authors' best knowledge, this is the first DNS study of isolated turbulent premixed cool flames in non-autoignitive conditions.

The flame properties and turbulence parameters for all cases considered are listed in Table 1. In Cases 1–4, the equivalence ratio (ϕ) is fixed at 1, while the non-dimensional turbulent intensity (u'/S_L) is increased from 2 to 8 to investigate turbulent cool flames at different turbulence intensities. In Cases 5 and 6, the equivalence ratio is decreased and increased respectively at fixed u'/S_L=6. Therefore, Cases 3, 5, and 6 form an equivalence ratio sweep. In all cases, the non-dimensional integral length scale (l_T/l_f) is fixed to 2. Here, S_L is the laminar cool flame speed and l_f is the laminar cool flame thickness computed based on the maximum temperature gradient. The corresponding Damköhler

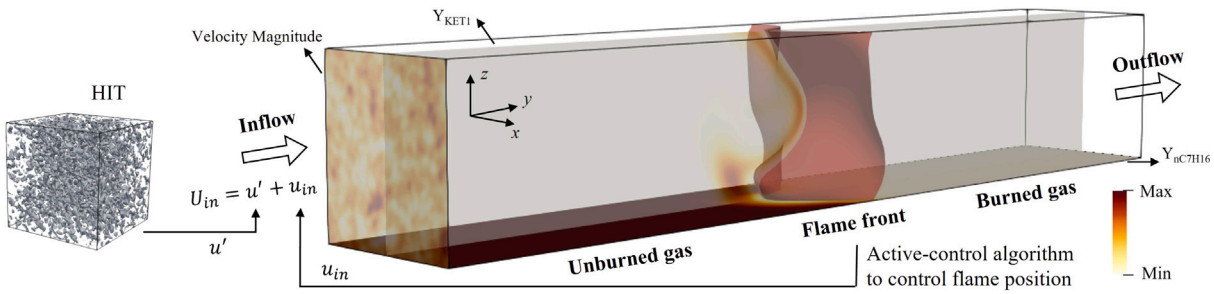

Fig. 1. Computational case setup of DNS. The inlet flow velocity U_{in} consists of the mean u_{in} and fluctuation u' parts. The flame front which is colored in red is denoted by the temperature iso-surface. The velocity magnitude distribution at the inlet, the Y_{nC7H16} distribution in the horizontal bottom cutting plane, and the Y_{KET1} distribution in the vertical central cutting plane are also presented. (For interpretation of the references to color in this figure legend, the reader is referred to the web version of this article.)

Table 1
Flame properties and turbulence parameters for cases considered. S_L is the laminar flame speed, $l_f = (T_b - T_u)/|\nabla T|_{max}$ is the laminar flame thickness, δ is the laminar reaction zone thickness which is defined as the width of region with fuel consumption rate exceeding 20% of the peak value, u' is the turbulent fluctuation speed, l_T is the turbulent integral length scale, $Da = (l_T/u')/(l_f/S_L)$ is the Damköhler number, $Ka = (l_f/S_L)(u'^3/(\nu l_T))^{1/2}$ is the Karlovitz number, Ka_δ is the reaction zone Karlovitz number, $Re_T = u' l_T/\nu$ is the turbulent Reynolds number, and $\tau_e = l_T/u'$ is the eddy turn over time. Here, ν is the kinematic viscosity of unburned gas. All parameters of the corresponding laminar flames are computed using Cantera [17].

Cases	ϕ	S_L [m/s]	l_f [mm]	δ [mm]	u'/S_L	l_T/l_f	Da	Ka	Ka_δ	Re_T	τ_e [ms]
1	1.0	0.29	1.32	1.05	2.0	2.0	1.00	4.33	1.98	18.72	3.26
2	1.0	0.29	1.32	1.05	4.0	2.0	0.50	12.24	5.60	37.44	1.16
3	1.0	0.29	1.32	1.05	6.0	2.0	0.33	22.48	10.29	56.16	0.62
4	1.0	0.29	1.32	1.05	8.0	2.0	0.25	34.61	15.84	74.88	0.41
5	0.6	0.28	1.57	1.42	6.0	2.0	0.33	23.07	15.96	59.16	0.76
6	2.0	0.27	1.01	0.58	6.0	2.0	0.33	21.42	4.86	51.01	0.49

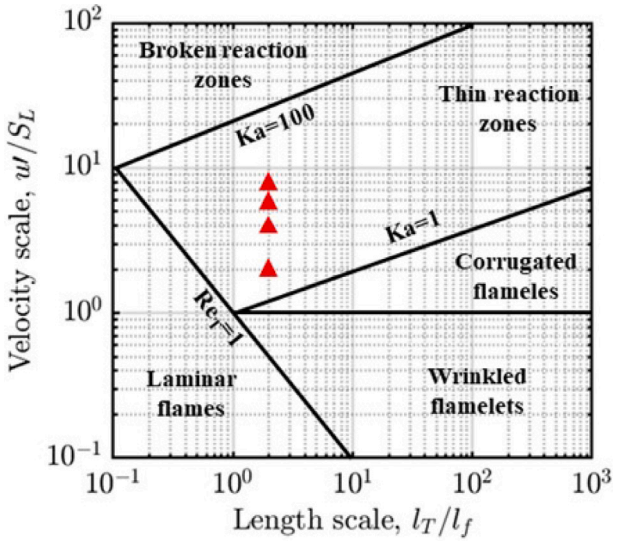

Fig. 2. Turbulent cool flame cases in Peter's regime diagram [25]. Note that cases with different equivalence ratios overlap in the diagram.

number Da, Karlovitz number Ka, and turbulence Reynolds number Re_T are also reported in Table 1. Note that all cases are located in the thin reaction zone in Peters' regime diagram [25], as shown in Fig. 2. Besides, as the reaction zone Karlovitz number (Ka_δ) was reported to be more relevant for the transition to distributed burning [19], Table 1 also presents Ka_δ for all cases, which is calculated as $Ka_\delta = \delta^2/\eta_\delta^2$ [19], where δ is the laminar reaction zone thickness and η_δ is Kolmogorov length scale evaluated at the reaction zone (taken at the temperature corresponding to the peak fuel consumption rate in the laminar flame).

The computational domain is determined by L=5.3l_T and is discretized by an uniform Cartesian grid of $N \times 6N \times N$ with N=128. Consequently, the cool flame thickness is always resolved by more than 12 grid points and the criterion of $k_{max}\eta > 2.5$, where $k_{max} = \pi N/L$ is the maximum wavenumber magnitude in DNS and η is the Kolmogorov length scale, is satisfied for all cases. A grid convergence study is provided in Supplementary Material. The time step in the simulation is about 1×10^{-6} s, corresponding to CFL=0.3. The simulated time is about 70 eddy turnover time (τ_e) for most cases except for Case 1 where the simulated time is 40 τ_e. It takes 600 hours for each DNS case when using 432 CPUs.

2.3. Reference laminar cool flames

To provide basic understandings of the laminar cool flame structure, Fig. 3 shows the profiles of temperature, mass fractions of reactant (n-C_7H_{16}), product (CH_2O), and intermediate species (C_7H_{15} and KET1, i.e., ketohydroperoxide), as well as the fuel consumption rate ($\dot{\omega}_F$) for the reference laminar cool flames at different equivalence ratios. It is seen that for all equivalence ratios, the reactant is only partially consumed and the burned temperature is very low (<1000 K), which are typical characteristics of cool flames as reported in many previous studies [1]. Besides, it is noted that the reaction zone for cool flames is much wider compared with hot flames, which can be seen from the mass fraction distributions of intermediate species and fuel consumption rate. In particular, the reaction zone width δ, which is defined as the width of the region with fuel consumption rate higher than 20% of the peak value [16], is found to be comparable with laminar flame thickness l_f (see in Table 1). Besides, compared with δ, the reaction zone characterized by mass fractions of the intermediate species is even thicker. These features would substantially influence the interaction between cool flames and turbulence.

3. Results and discussion

3.1. Structure of turbulent premixed cool flames

Fig. 4 first shows the structure of turbulent premixed cool flame in physical space at different turbulent intensities, by plotting contours of temperature, mass fractions of CH_2O, C_7H_{15}, and KET1, as well as the normalized fuel consumption rate ($\dot{\omega}_F/\dot{\omega}_{F,L,max}$, where $\dot{\omega}_{F,L,max}$ is the peak value of fuel consumption rate in the corresponding 1D laminar flame) on the 2D vertical central slice. For Case 1 with u'/S_L=2, the

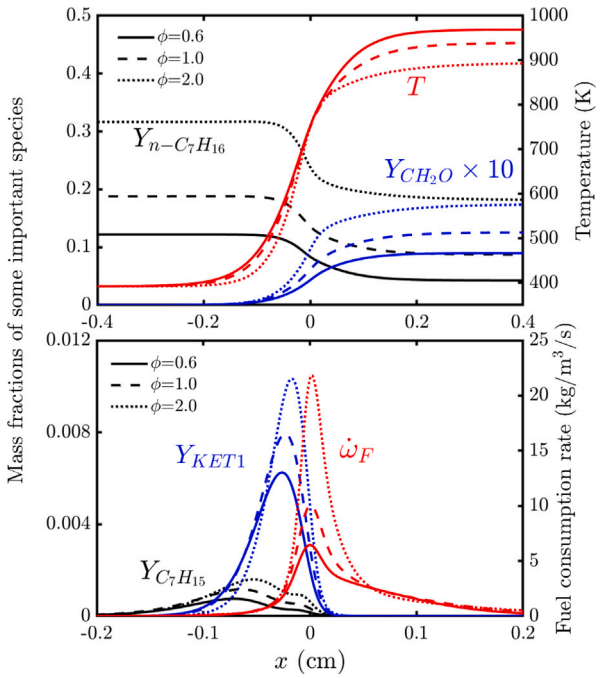

Fig. 3. Spatial profiles of temperature, mass fractions of n-C_7H_{16}, CH_2O, C_7H_{15}, and KET1, as well as the fuel consumption rate ($\dot{\omega}_F$) for the reference laminar cool flames at different equivalence ratios.

Table 2
Time averaged δ_T/δ for Cases 1–4.

Cases	1	2	3	4
δ_T/δ	2.42	3.13	3.71	3.82

cool flame front is wrinkled by the large turbulence eddies while the local flame front still resembles the 'flamelet' structure in general. With increasing u'/S_L, the cool flame is strongly distorted and some flame pockets of burned gas are formed due to the flame-to-flame interactions. Consequently, the turbulent cool flame brush is significantly thickened with distributed reaction zone for Cases 3 and 4. Specifically, certain amounts of C_7H_{15} and KET1 are observed in low temperature region, while the fuel consumption rate tends to be distributed in the high temperature region. To quantify the distributedness of the reaction zone, the ratio of the turbulent reaction zone thickness δ_T=Vol($\dot{\omega}_F > 0.2\dot{\omega}_{F,L,max}$)/$A_L$ to that of the reference laminar flame δ is computed [16], although δ_T/δ does not distinguish between an increase in turbulent flame surface area and flame thickness. Note that δ_T/δ has also been computed based 0.1 threshold, and it is found that this ratio is not sensitive to the choice of threshold (see Supplementary Materials). As listed in Table 2, the time averaged δ_T/δ is noticeably larger than 1 and shows an increasing trend with u'/S_L, although these turbulent cool flames are still within the thin reaction zone in Peters' regime diagram. Besides, in [19] where the same fuel type (n-C_7H_{16}) was considered in the context of hot flames, the distributed flame structure was observed at a much higher Ka level (Ka >200) compared with this study. Fig. 5 further directly compares δ_T/δ at different Ka_δ between turbulent cool flames (Cases 1–4 in this work) and hot flames (Cases A–C in [19]). It is seen that the data points of cool flames are well above those of hot flame. This suggests that compared with hot flames, cool flames are more prone to be distributed by turbulence. This is due to the large reaction zone thickness of cool flame as shown in Table 1 and the small increase in temperature across the cool flame front. These results are consistent with the observation in [16].

On the other hand, it can also be seen from Fig. 4 that the local fuel consumption rate is largely altered along the flame front. Specifically, high fuel reactivity and high concentrations of intermediate species (C_7H_{15}, and KET1) are observed at the negatively stretched flame segments which are convex towards the burned gas, while low fuel reactivity and low concentrations of intermediate species are observed at positively stretched flame segments which are convex towards the fresh gas. This behavior is analogous to the turbulent hot flames of lean n-C_7H_{16}/air mixture whose Lewis number is larger than 1 as reported in [19], indicating that the differential diffusion effects are also important for turbulent cool flames, even at high turbulent intensities.

To investigate the turbulent cool flame structure in temperature space, Fig. 6 shows the joint probability density functions (PDFs) and conditional means of $Y_{C_7H_{15}}$, Y_{CH_2O}, Y_{KET1}, and $\dot{\omega}_F$ versus temperature (T) for Cases 1–4. The corresponding 1D laminar flamelet with mixture-averaged transport model and unity Lewis number model are also plotted for comparison. The comparison between these two 1D laminar flamelets indicates that the differential diffusion has strong influence on the distributions of $Y_{C_7H_{15}}$, Y_{KET1}, and $\dot{\omega}_F$. For $Y_{C_7H_{15}}$, the conditioned mean profile of turbulent cool flames falls within the region enveloped by the two 1D flame flamelets and show considerable departure from them. For Y_{KET1}, the conditioned mean profile is close to the unity Lewis number 1D flamelet in the low temperature region while it is approaching the non-unity Lewis number 1D flamelet in the relatively high temperature region. In contrast, for Y_{CH_2O}, the conditioned mean profile of turbulent flames overlaps with the two 1D flame solutions. Regarding $\dot{\omega}_F$, although the mean profile follows the non-unity Lewis number 1D flamelet in low temperature region, its peak value is reduced, approaching the peak value of unity Lewis number 1D flamelet. Such reduction in peak fuel consumption rate by turbulence was also reported for turbulent lean n-C_7H_{16}/air hot flames in [19].

However, it is interesting to note from Fig. 6 that the turbulent cool flame structure in the temperature space shows a very weak sensitivity to the turbulence intensity as the mean profiles are very similar at different turbulence intensities for all quantities. This is further confirmed by Fig. 7 where conditioned mean profiles of Y_{KET1} and $\dot{\omega}_F$ for Cases 1–4 are directly compared. Here, the data was extracted only from the iso-surface of temperature which corresponds to the maximum heat release rate in 1D flamelet. It is seen that the profiles at different turbulence intensities almost collapse with each other. This observation serves as a evidence indirectly supporting that the LTC chemical pathways which govern the cool flame dynamics are globally insensitive to turbulence as reported in [16].

3.2. Global turbulent cool flame speed

In this subsection, the global flame dynamics of turbulent premixed cool flames are investigated. To characterize the global propagation speed of turbulent cool flames, the turbulent burning velocity S_T is computed based on the fuel consumption rate as:

$$S_T = \frac{1}{\rho_u(Y_{F,u} - Y_{F,b})A_L}\int_\Omega \dot{\omega}_F dV \tag{1}$$

where ρ_u is the unburned gas density, $Y_{F,u}$ and $Y_{F,b}$ are the mass fraction of fuel species in unburned gas and burned gas, respectively, $A_L = L\times L$ is the projected flame area in the streamwise direction, and Ω is the volume of the whole computational domain. The turbulent cool flame surface area A_T is computed based on the generalized flame surface density $\Sigma = |\nabla c|$ as:

$$A_T = \int_\Omega \Sigma dV = \int_\Omega |\nabla c| dV \tag{2}$$

where c=($Y_{F,u}$-Y_F)/($Y_{F,u}$-$Y_{F,b}$) is the progress variable and Y_F is the mass fraction of n-C_7H_{16}. The stretching factor I_0 is then introduced to characterize the deviation of local fuel consumption rate as:

$$\frac{S_T}{S_L} = I_0\frac{A_T}{A_L}. \tag{3}$$

Thus, I_0 can be calculated as $I_0 = (S_T/S_L)/(A_T/A_L)$, which measures the impact of differential diffusion.

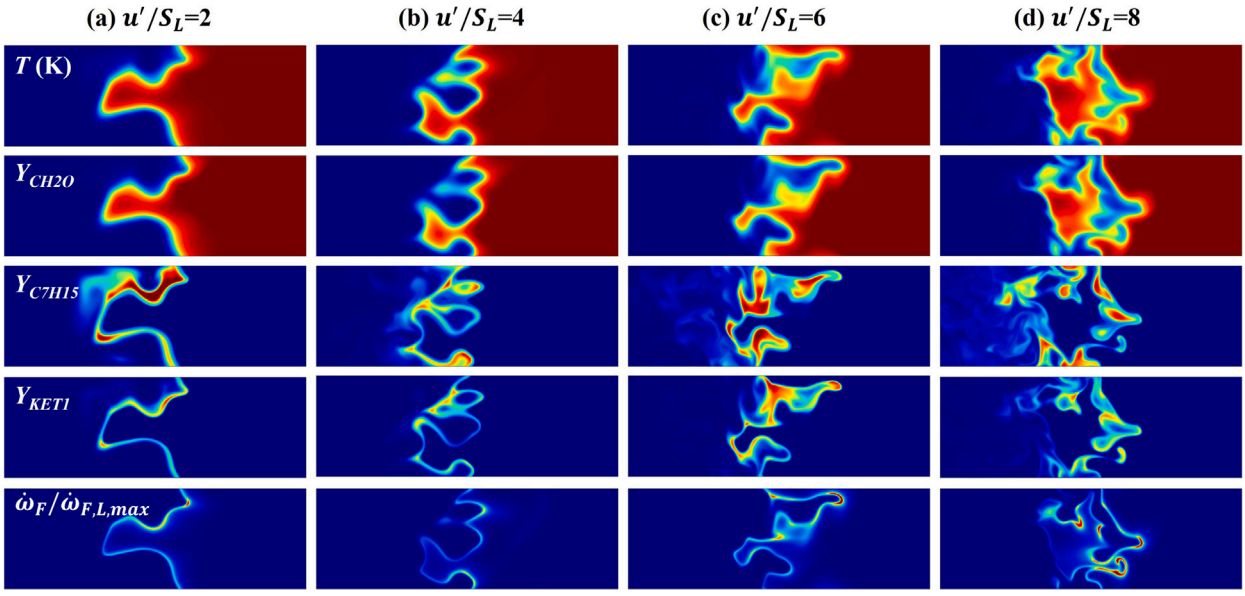

Fig. 4. 2D slices of $3L \times L$ region centered around the flames showing the contours of temperature (T), mass fractions of CH_2O, C_7H_{15}, and KET1, as well as the normalized fuel consumption rate ($\dot{\omega}_F/\dot{\omega}_{F,L,max}$), for Cases 1–3 with increasing u'/S_L. The ranges for T, Y_{CH_2O}, $Y_{C_7H_{15}}$, Y_{KET1}, and $\dot{\omega}_F/\dot{\omega}_{F,L,max}$ are [392, 938 K], [0, 0.012], [0 0.0013], [0, 0.015], and [0, 2], respectively.

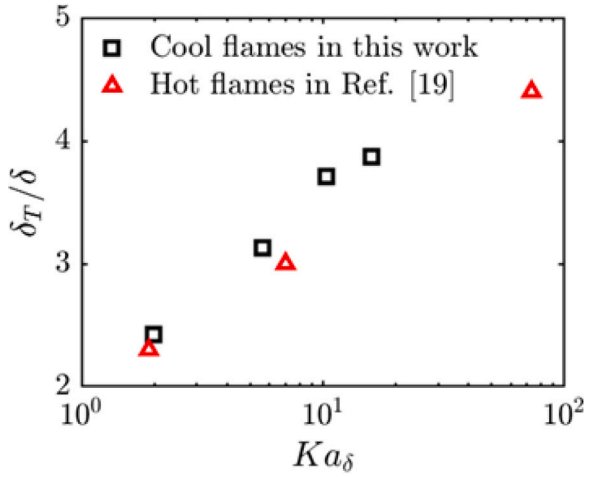

Fig. 5. Change of δ_T/δ with Ka_δ for turbulent cool flames (Cases 1–4 in this work) and hot flames (Cases A–C in [19]).

Fig. 8 exemplarily shows the temporal evolution of S_T/S_L, A_T/A_L, and I_0 for Case 1 with ϕ=3 and u'/S_L=2. It can be seen that S_T/S_L starts from 1, and undergoes a sharp increase as the generated turbulence wrinkles the cool flame front. Meanwhile, I_0 is decreased to a value lower than 1 due to perturbation of local reactivity. Once the turbulence reaches the prescribed level, S_T/S_L fluctuates around a mean value. Despite the oscillation, the turbulent cool flame has reached the statistically steady state after $t > 20\tau_e$. Therefore, for all cases, the statistics are collected after $t > 20\tau_e$ and over a period of at least $20\tau_e$ as indicated by the horizontal lines in Fig. 8. Results for all other cases can be found in Supplementary Material.

Fig. 9 shows the time averaged S_T/S_L, A_T/A_L, and I_0 at different u'/S_L. It is found that with increasing u'/S_L, S_T/S_L increases substantially, which is attributed to the increase in A_T/A_L. This aligns with the thickened turbulent cool flame brush shown in Fig. 4 and Table 2. In contrast, I_0 is lower than 1, indicating that the differential diffusion exerts a suppression effect on the propagation of turbulent cool flames, which is consistent with the reduction in fuel consumption rate observed in Fig. 7. Moreover, I_0 is not sensitive to the turbulence intensity and remains almost constant at about 0.63, which is consistent with the fact that the turbulent cool flame structure in the temperature space is insensitive to the turbulence intensity as discussed in the previous subsection. In the next subsection, the local flame dynamics analysis will be conducted to better explain the variation trend of turbulent cool flame speed.

3.3. Local dynamics of turbulent cool flames

In this subsection, the local turbulence-chemistry interaction of turbulent cool flames are analyzed in terms of the flame displacement speed S_d and flame stretch rate K_S. The latter will not only influence the local flame speed by coupling with differential diffusion but also control the turbulent flame surface generation since $K_S = 1/A_T(dA_T/dt)$ by definition.

The flame displacement speed S_d can be decomposed into three components as:

$$S_d = S_{d,r} + S_{d,n} + S_{d,t} \tag{4}$$

where $S_{d,r} = \dot{\omega}_c/\rho|\nabla c|$, $S_{d,n} = \mathbf{n} \cdot \nabla(\rho D \mathbf{n} \cdot \nabla c)/\rho|\nabla c|$, and $S_{d,t} = -2D\kappa$ are the reaction, normal diffusion, and tangential diffusion components of S_d, respectively. Here, $\dot{\omega}_c$ is the reaction rate of progress variable, $\mathbf{n} = -\nabla c/|\nabla c|$ the flame normal vector that points toward the unburned gas, $\kappa = 0.5(\nabla \cdot \mathbf{n})$ is the flame front curvature, D is the progress variable diffusivity.

The stretch rate K_S can be decomposed into two components as:

$$K_S = a_t + 2\kappa S_d, \tag{5}$$

where $a_t = \nabla \cdot \mathbf{u} - \mathbf{nn} : \nabla \mathbf{u}$ is the tangential strain rate, and $2\kappa S_d$ is the curvature stretch. Accordingly, the stretch Karlovitz number is computed as $Ka_S = Ka_{S,t} + Ka_{S,c}$ with $Ka_{S,t} = (l_f/S_L)a_t$ and $Ka_{S,c} = (l_f/S_L)2\kappa S_d$. All these quantities are evaluated at the flame front that is characterized by the iso-surface of progress variable corresponding to the maximum fuel consumption rate in the reference laminar cool flames.

Fig. 10 shows the PDF of density-weighted $S_d^* = \rho S_d/\rho_u$ and its components for Cases 1–4. In Case 1, the PDF of S_d^* is found to peak approximately at S_L, indicating that the local cool flame front is still burning similar to a laminar flamelet. In Cases 2–4 with relatively high

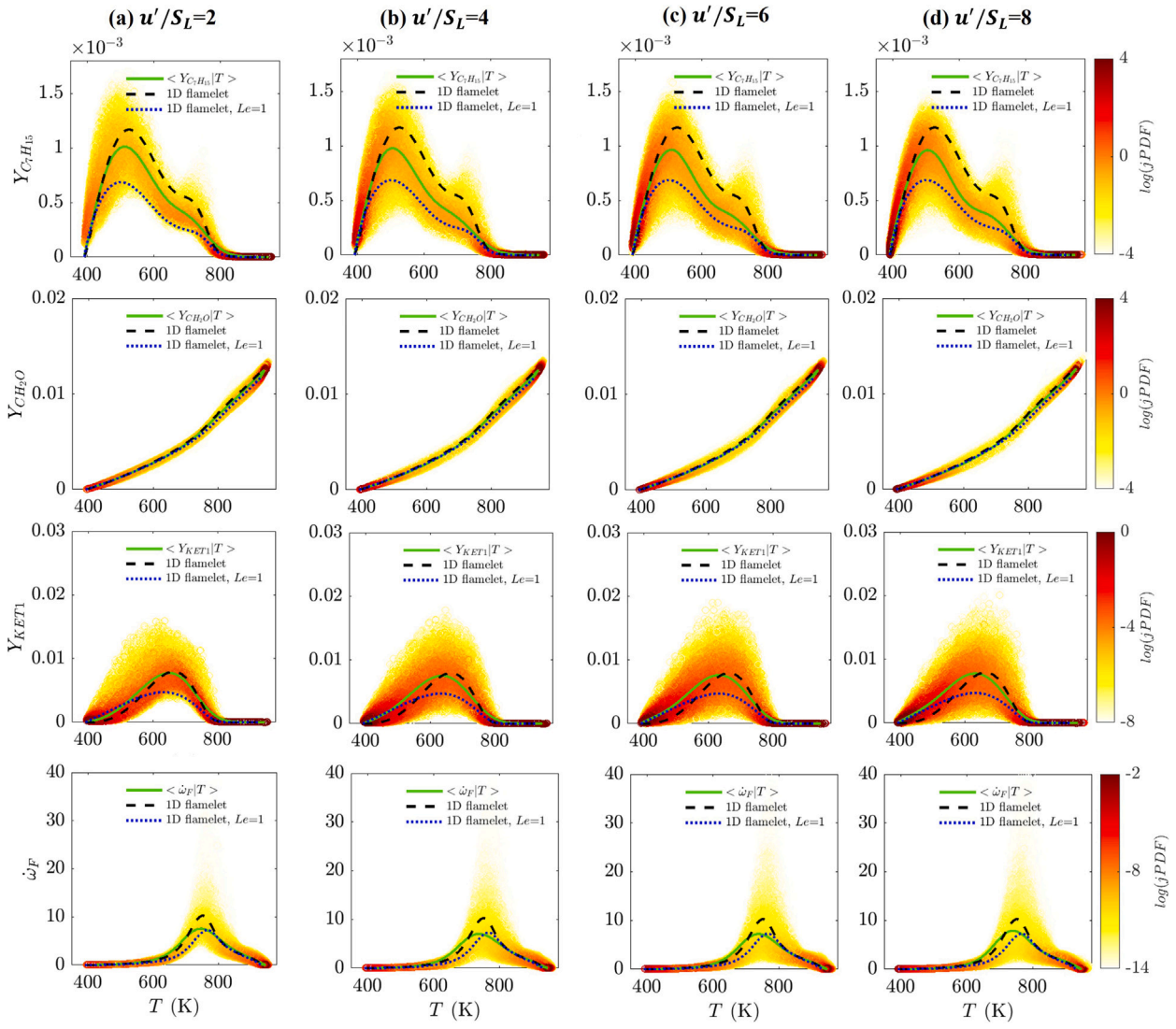

Fig. 6. Joint PDFs (contours) and conditioned mean (green solid lines) of $Y_{C_7H_{15}}$, Y_{CH_2O}, Y_{KET1}, and $\dot{\omega}_F$ versus temperature for Cases 1–4 with increasing u'/S_L, in comparison with the corresponding 1D laminar flame solutions with mixture-averaged model (dashed lines) and unity-Le model (dotted lines). (For interpretation of the references to color in this figure legend, the reader is referred to the web version of this article.)

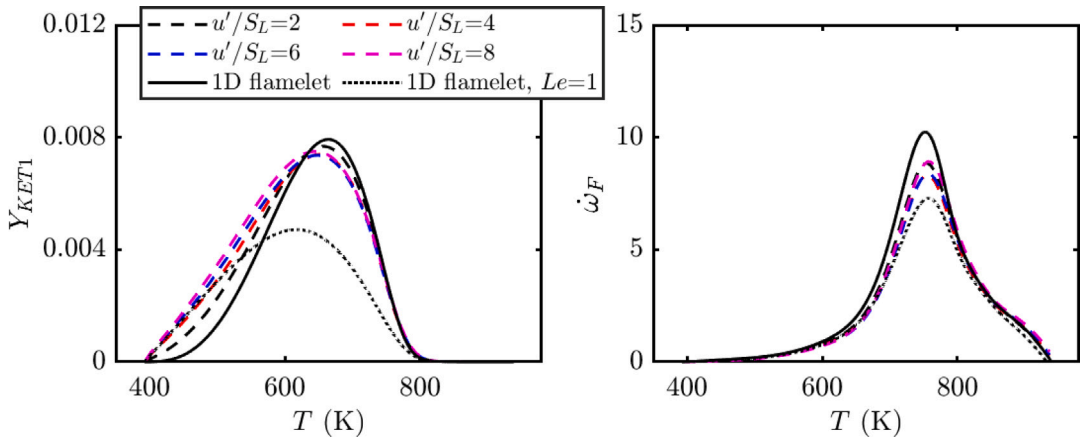

Fig. 7. Conditioned mean profiles of Y_{KET1} and $\dot{\omega}_F$ on temperature space for Cases 1–4. The corresponding 1D laminar flamelets are also plotted for reference. The data was extracted only from the iso-surface of temperature which corresponds to the maximum heat release rate in 1D flamelet.

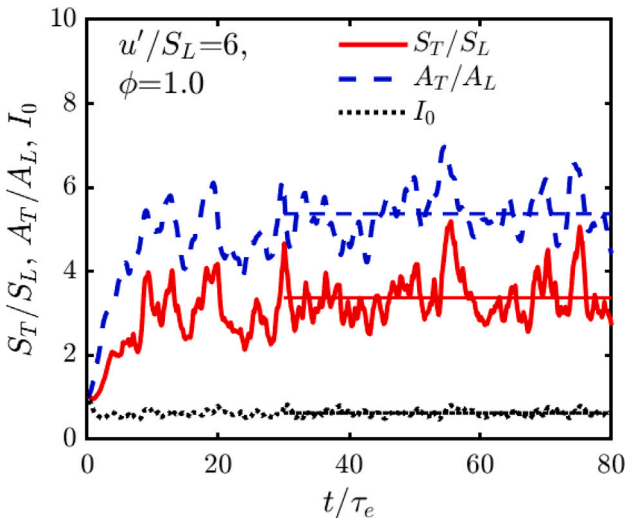

Fig. 8. Temporal evolution of the S_T/S_L, A_T/A_L and I_0 for Case 3 with ϕ=1 and u'/S_L=6. The time is normalized by the eddy turnover time τ_e. The corresponding horizontal lines are time averaged values.

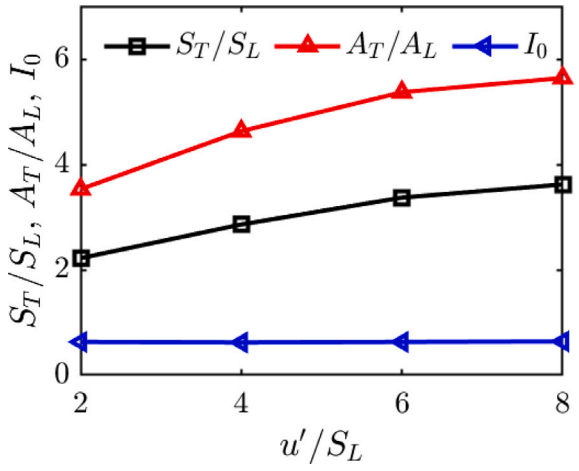

Fig. 9. Change of time-averaged S_T/S_L, A_T/A_L, and I_0 with u'/S_L.

u'/S_L, $S^*_{d,r}$ shifts leftwards and shows a longer tail in large positive value, which is resulted from the enhanced differential diffusion and also turbulence fluctuation, while $S^*_{d,n}$ shifts to positive side (towards zero) with increasing u'/S_L. As for $S^*_{d,t}$, it peaks at zero value with generally good symmetry for all cases and spans a slightly wider range with increasing u'/S_L due to the enhanced turbulence fluctuation. According to the definitions of $S^*_{d,n}$ and $S^*_{d,t}$ in Eq. (4), $S^*_{d,n}$ is proportional to the gradient of progress variable, while $S^*_{d,t}$ is proportional to the curvature. At higher u'/S_L, the turbulent cool flame is widened, leading to smaller gradient of progress variable and thus smaller magnitude of $S^*_{d,n}$. In contrast, u'/S_L only marginally influences the PDF of curvature (which will be shown below) and thus $S^*_{d,t}$ is insensitive to u'/S_L. Consequently, S^*_d spans a much wider range to both negative and positive sides in Cases 2–4 compared with Case 1. This is consistent with the thickened flame brush of turbulent cool flames for Cases 2–4 as observed in Fig. 4.

To examine the dependence of S_d on the flame tangential strain (a_t) and curvature (κ), Fig. 11 presents the joint PDF of S^*_d/S_L against $Ka_{S,t}$ and S^*_d/S_L against $\kappa * l_f$. It is found that at all turbulence intensities, S^*_d/S_L is more strongly correlated with $\kappa * l_f$ compared with $Ka_{S,t}$, indicating that for the turbulent premixed cool flames, the local flame speed is primarily influenced by the flame curvature instead of tangential strain rate. Specifically, S^*_d/S_L is negatively correlated with $\kappa * l_f$ in both positive and negative $\kappa * l_f$ regions, while there is no obvious correlation between S^*_d/S_L and $Ka_{S,t}$. Besides, the joint PDF of S^*_d/S_L against $\kappa * l_f$ tends to peak at ($\kappa * l_f$=0, S^*_d/S_L=1) even for the highest turbulent intensity case. This further confirms that S^*_d/S_L is mainly controlled by flame curvature, instead of flame tangential strain. Such strong negative correlation between local reactivity and curvature was also observed for turbulent lean n-C_7H_{16}/air hot flames in [19], which once again indicates that the turbulent premixed cool flame is analogous to the turbulent hot flame with the effective Lewis number larger than 1. Furthermore, to demonstrate the influence of differential diffusion (due to Lewis number larger than 1) on the cool flame dynamics, we conducted an additional DNS case with unity Lewis number based on Case 3. As shown in Supplementary Material, when the Lewis number is set to be 1, I_0 is close to 1 and the strong negative correlation between $S^*_{d,r}/S_L$ and $\kappa * l_f$ has disappeared.

To better understand the correlation between S^*_d/S_L and $\kappa * l_f$, Fig. 12 shows the mean values of S^*_d/S_L and its components conditioned on $\kappa * l_f$. First, it can be seen that S^*_d/S_L shows a similar negative correlation with $\kappa * l_f$ at different turbulence intensities, which is attributed to the similar dependence of $S^*_{d,r}/S_L$ and $S^*_{d,t}/S_L$ on $\kappa * l_f$. The latter is expected given $S_{d,t} = -2D\kappa$ where D is not relevant with turbulence intensity. Second, in the negative curvature region, S^*_d/S_L is primarily determined by the behavior of reaction component $S^*_{d,r}/S_L$, while in the positive curvature region, $S^*_{d,r}/S_L$ approaches zero and thus S^*_d/S_L is primarily determined by the tangential diffusion component $S^*_{d,t}/S_L$. Third, due to different sensitivities of $S^*_{d,r}/S_L$ and $S^*_{d,t}/S_L$ to $\kappa * l_f$, S^*_d/S_L shows a stronger correlation with $\kappa * l_f$ in the negative curvature region than in the positive curvature region. Finally, it is worth noting that the magnitude of $S^*_{d,t}/S_L$ is comparable to or even higher at large $\kappa * l_f$ region than that of $S^*_{d,n}/S_L$, suggesting the important role of the tangential diffusion, which should not be neglected when modeling turbulent premixed cool flames.

Fig. 13 further shows the PDF of Ka_S and its components as well as the normalized κ. It is found that with increasing u'/S_L, the PDF of Ka_S spans a much wider range and shifts rightwards. This is largely resulted from the dependence of the tangential strain rate term $Ka_{S,t}$ to turbulence intensity. In contrast, the PDF of the curvature term $Ka_{S,c}$ shows a weak sensitivity to u'/S_L and peaks at zero. This is because the PDF of curvature is only slightly influenced by u'/S_L and features a symmetry profile centered on κ=0. These results indicate that the increasing trend of A_T/A_L with u'/S_L for cool flames is mainly attributed to the enhanced tangential strain rate. On the other hand, considering that the local flame displacement speed is mainly controlled by the flame curvature as discussed above, the weak dependence of flame curvature on u'/S_L explains the almost constant I_0 at different turbulence intensities observed in Fig. 9.

To summarize, in this subsection, the local flame dynamics analysis has been conducted to better understand the global behavior of turbulent premixed cool flames. On the one hand, the local flame displacement speed is found to be strongly negatively correlated with the flame curvature and neither such negative correlation nor the distribution of flame curvature is sensitive to the turbulence intensities. This results in sub-unity I_0 and its insensitivity to turbulence intensity. On the other hand, the PDF of the tangential strain rate is found to span a much wider range and shift to the positive side as u'/S_L increases, suggesting that the enhanced tangential strain rate is the main cause of the increase in surface area (A_T) of the turbulent cool flames.

Note that in [16], I_0 was found to be larger than 1 for turbulent premixed cool flames, which was attributed to the combination of a thickening of the reaction zone and a slight increase of the burning rate in temperature space compared with the reference laminar flame. However, in this study I_0 <0 was observed, and the fuel reaction rate of turbulent cool flames was found to be significantly lower than its laminar counterpart (see Fig. 6). Such difference in turbulence-chemistry

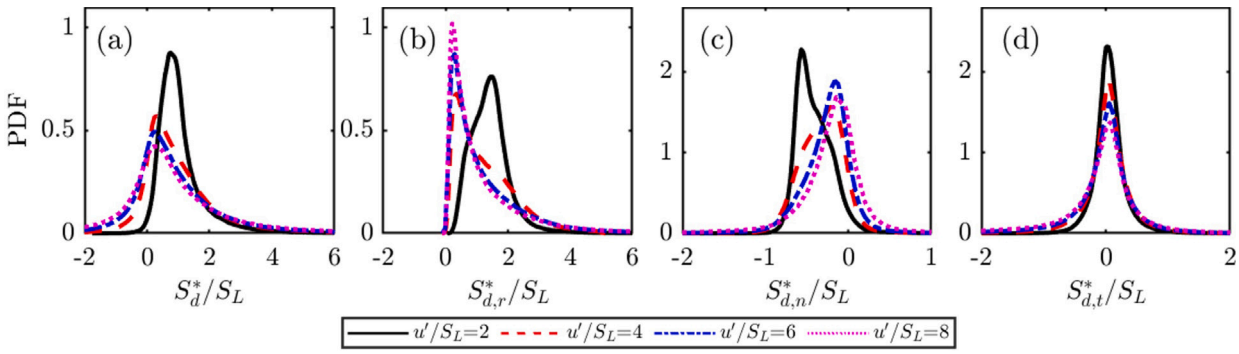

Fig. 10. PDF of normalized S_d^*/S_L and its components for Cases 1–4.

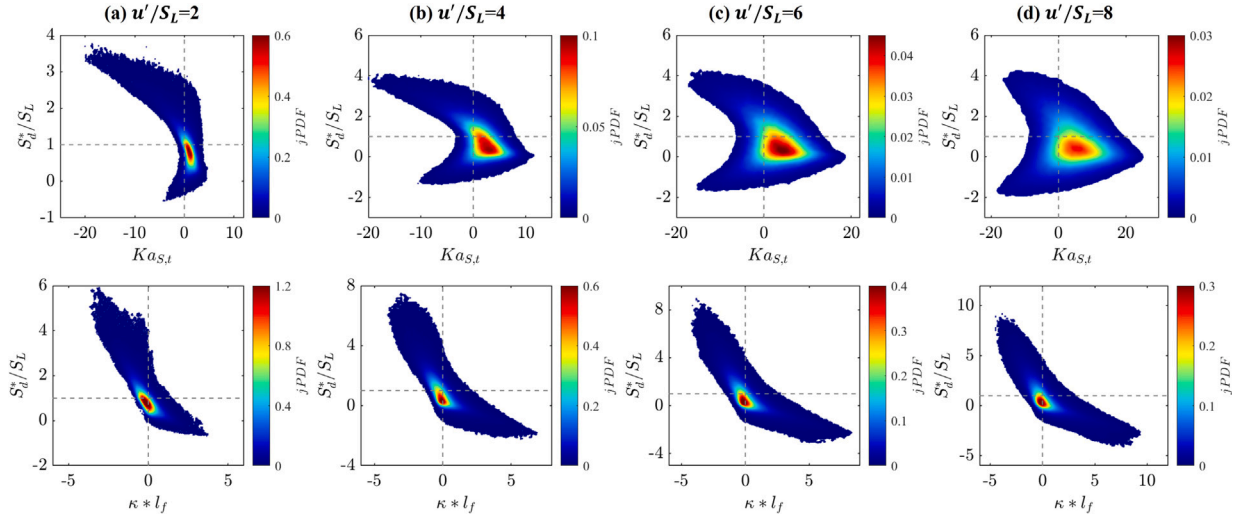

Fig. 11. Joint PDF of S_d^*/S_L vs. $Ka_{S,t}$ (top) and S_d^*/S_L vs. $\kappa * l_f$ (bottom) for Cases 1–4.

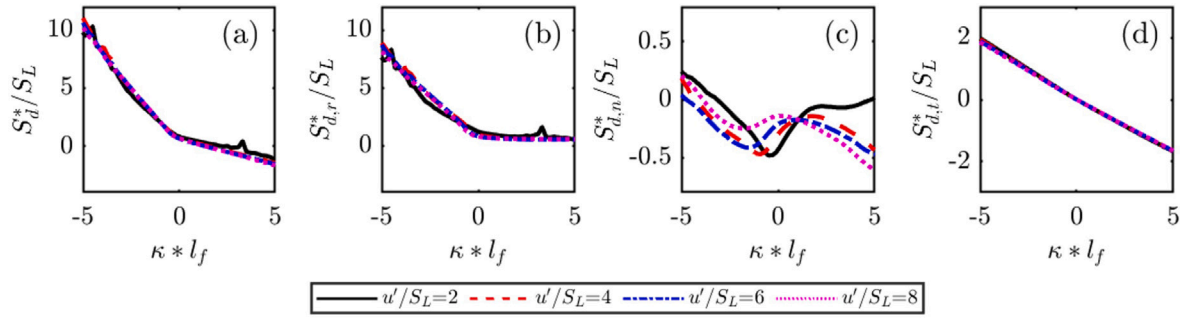

Fig. 12. Conditioned mean S_d^*/S_L and its components with $\kappa * l_f$ for Cases 1–4.

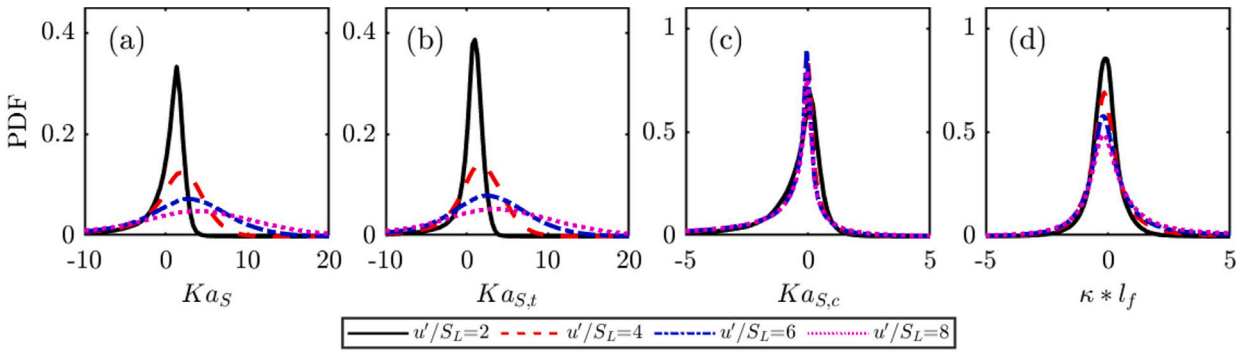

Fig. 13. PDF of Ka_S and its components, as well as $\kappa * l_f$ for Cases 1–4.

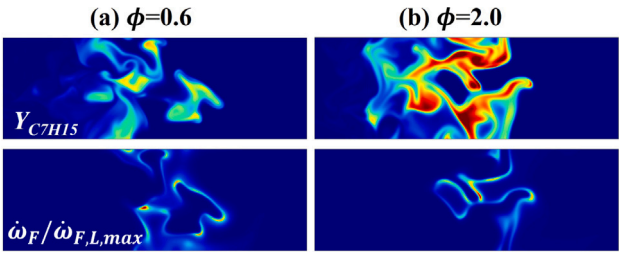

Fig. 14. 2D slices of $3L \times L$ region centered around the flames showing the contours of mass fraction of C_7H_{15} and the normalized fuel consumption rate ($\dot{\omega}_F/\dot{\omega}_{F,L,max}$), for Case 5 and 6. The ranges for $Y_{C_7H_{15}}$ and $\dot{\omega}_F/\dot{\omega}_{F,L,max}$ are identical to those used in Fig. 4 for fair comparison.

interaction are potentially due to the different thermodynamic conditions (autoignitive condition in [16] vs. non-autoignitive condition in the present study). Therefore, it merits further study on the cool flame dynamics at a wide range of temperature and pressure, which will be the focus of our future work.

3.4. Effects of equivalence ratio

In this section, the flame structure, global flame propagation speed, and the local flame dynamics of turbulent premixed cool flames with different equivalence ratios are compared to examine whether the above findings are sensitive to the equivalence ratio.

Figs. 14 and 15 first show the structure of turbulent premixed cool flames for Cases 5 (ϕ=0.6) and Case 6 (ϕ=2.0) in physical space and temperature space, respectively. Note that only the structures of $Y_{C_7H_{15}}$ and $\dot{\omega}_F/\dot{\omega}_{F,L,max}$ are presented for brevity. By comparing Fig. 14 with Fig. 4, it is found that the turbulent cool flame brush is thickened by turbulence in a similar level for different equivalence ratios, although the magnitudes of $Y_{C_7H_{15}}$ and $\dot{\omega}_F$ are different. The latter results from the differences in laminar premixed cool flames shown in Fig. 3, rather than the turbulence-chemistry interaction. Regarding the flame structure in temperature space, the influence of turbulence is found to be similar among different equivalence ratio, by comparing Fig. 15 with Fig. 6. Specifically, regardless of the equivalence ratio, the conditioned mean profile of $Y_{C_7H_{15}}$ falls within the region enveloped by the 1D flamelet solutions, while the mean profile of $\dot{\omega}_F$ follows the 1D non-unity Lewis number flamelet in the low temperature region and the peak value is reduced to approach the peak value of 1D unity Lewis number flamelet.

Table 3 lists the time averaged S_T/S_L, A_T/A_L, and I_0 for Cases 3, 5, and 6 to compare the global flame speed of turbulent premixed cool flames with different equivalence ratios. It is found that A_T/A_L and I_0 are relatively insensitive to the equivalence ratio, leading to a nearly constant S_T/S_L at different equivalence ratios. It is worth mentioning that I_0 <1 at all three equivalence ratios indicates that the Markstein number of cool flame is positive regardless of the equivalence ratio, which is consistent with the negative correlation between flame speed and stretch rate observed in previous laminar cool flame studies [9,10]. Moreover, I_0 <1 also implies that the effective Lewis number of cool flames is always larger than 1 for equivalence ratio ranging from 0.6–2.0. Therefore, most definitions of effective Lewis number developed for hot flames cannot be readily applied to cool flames.

A potential reason for such dilemma may lie in the improper definition of equivalence ratio for cool flames. Generally, the equivalence ratio (ϕ) is defined as:

$$\phi = (\frac{Y_{F,u}}{Y_{O,u}})/(\frac{Y_F}{Y_O})_{st}, \tag{6}$$

where $Y_{F,u}/Y_{O,u}$ is the fuel and oxidizer mass ratio in the unburned mixture, and $(Y_F/Y_O)_{st}$ is the stoichiometric mass ratio. Here, $(Y_F/Y_O)_{st}$ is calculated based on the global 1-step reaction where the fuel and

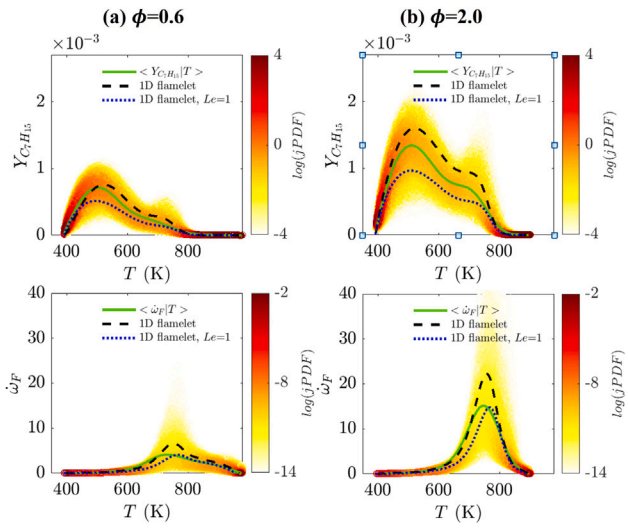

Fig. 15. Joint PDFs (contours) and conditioned mean (green solid lines) of $Y_{C_7H_{15}}$ and $\dot{\omega}_F$ versus temperature for Cases 5 and 6, in comparison with the corresponding 1D laminar flame solutions with mixture-averaged model (dashed lines) and unity-Le model (dotted lines). (For interpretation of the references to color in this figure legend, the reader is referred to the web version of this article.)

Table 3
Time averaged S_T/S_L, A_T/A_L, and I_0 for Cases 3, 5, and 6.

Cases	ϕ	S_T/S_L	A_T/A_L	I_0
5	0.6	3.37	5.37	0.63
3	1.0	3.33	5.39	0.61
6	2.0	3.34	5.13	0.65

oxidizer are fully consumed and converted into products (such as CO_2 and H_2O). However, for cool flames, neither the fuel nor the oxidizer has been fully consumed and the products are also different. Therefore, the conventional definition of $(Y_F/Y_O)_{st}$ is not suitable for cool flames. Considering that there is not a well-defined global 1-step reaction for cool flame chemistry, an alternative is to calculate $(Y_F/Y_O)_{st}$ of cool flames from the 1D unstretched laminar cool flame solutions as:

$$(\frac{Y_F}{Y_O})_{st,cool} = \frac{Y_{F,u} - Y_{F,b}}{Y_{O,u} - Y_{O,b}}, \tag{7}$$

where the subscripts "u" and "b" denote the unburned and burned gas, respectively. Then, the equivalence ratio of cool flame (ϕ_{cool}) can be computed as:

$$\phi_{cool} = (\frac{Y_{F,u}}{Y_{O,u}})/(\frac{Y_F}{Y_O})_{st,cool} \tag{8}$$

Table 4 presents $(Y_F/Y_O)_{cool}$, ϕ_{cool}, and Le_{fuel} for cool flames at different equivalence ratios. It is seen that ϕ_{cool} is much smaller than 1 for all cool flames, indicating that they are actually very "lean". Moreover, since they are "lean" cool flames, it is reasonable to use the Lewis number of fuel (Le_{fuel}) to characterize the effective Lewis number. As shown in Table 4, Le_{fuel} are larger than 2 for all cool flames, which demonstrates that the effective Lewis number of cool flames is always larger than 1 for ϕ ranging from 0.6–2.0. The above analysis serves as a preliminary explanation. More detailed analysis should be conducted even in the laminar cool flame context, which however, is not within the scope of the present study.

Fig. 16 shows the PDFs of S_d^*/S_L and its components for Cases 3, 5 and 6 with different equivalence ratios. It is found that the PDF of reaction term $S_{d,r}^*/S_L$ shifts slightly rightwards with increasing ϕ, which is compensated by the leftwards shift in the PDF of the normal diffusion terms $S_{d,n}^*/S_L$, while the PDF of the tangential diffusion term $S_{d,n}^*/S_L$ remains unchanged. Consequently, the PDF of S_d^*/S_L is found

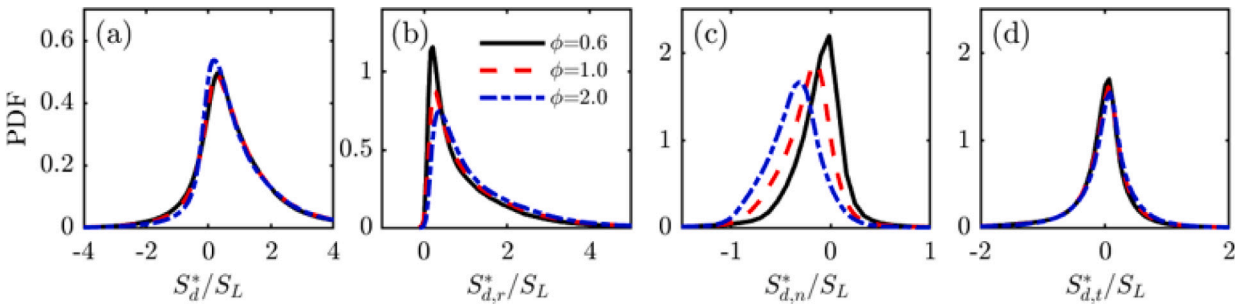

Fig. 16. PDF of S_d^*/S_L and its components for Cases 3, 5, and 6 with different equivalence ratios.

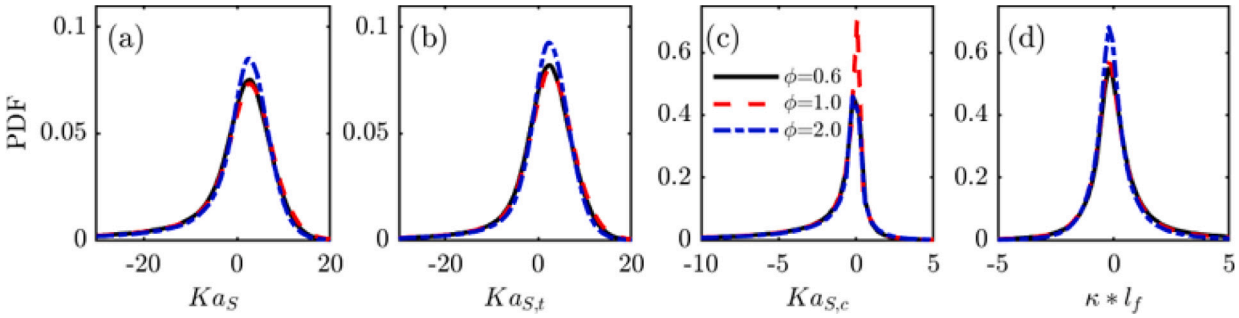

Fig. 17. PDF of Ka_S and its components, as well as $\kappa * l_f$ for Cases 3, 5, and 6 with different equivalence ratios.

Table 4
$(Y_F/Y_O)_{cool}$, ϕ_{cool}, and Le_{fuel} for cool flames at different equivalence ratios.

ϕ	$(Y_F/Y_O)_{cool}$	ϕ_{cool}	Le_{fuel}
0.6	1.11	0.15	2.70
1.0	1.24	0.23	2.50
2.0	1.40	0.41	2.17

to be similar for different equivalence ratios. Fig. 17 shows the PDFs of stretch rate Ka_S and its components, $Ka_{S,t}$ and $Ka_{S,c}$, as well as the curvature $\kappa * l_f$ for Cases 3, 5, and 6. Interestingly, all these quantities are found to be insensitive to the variation of ϕ. These results indicate that the flame-stretch interaction of local cool flame front is insensitive to the equivalence ratio, which is distinct from hot flames.

The above results suggest that those findings about the global and local flame dynamics of turbulent cool flames obtained in previous subsections still hold for different equivalence ratios. Moreover, additional six DNS cases that are identical to Cases 1–6 except for the normalized turbulence integral scale l_T/l_f=1 (rather than 2) are performed and analyzed to investigate whether the findings presented in this study are sensitive to turbulence integral scale. As shown in Supplementary Material, very similar results in terms of the influence of turbulence intensity and equivalence ratio on the flame structure and global and local flame dynamics are observed. In this context, the generality of these results are convincing, although further demonstration is needed given the limited thermodynamic condition considered in this study.

4. Conclusions

In this study, a series of direct numerical simulations of the statistically-planar turbulent premixed cool flames for n-$C_7H_{16}/O_2/O_3/N_2$ mixtures have been performed using detailed chemistry. The influences of turbulence intensity (u'/S_L) on the flame structure as well as the global and local flame dynamics were systematically investigated. Three main observations are made.

First, it is found that the turbulent cool flame brush is significantly thickened at high u'/S_L and the flame structure of turbulent premixed cool flames in the physical space is more prone to be distributed by turbulence compared with hot flames, due to the large reaction zone thickness of cool flames. As a result, the local flame reactivity along the flame front is largely altered by the differential diffusion effects. However, the turbulent cool flame structure in the temperature space only shows a weak sensitivity to u'/S_L, indicating that the LTC chemical pathways that govern the cool flame dynamics are globally insensitive to turbulence.

Second, with increasing u'/S_L, the normalized turbulent cool flame speed (S_T/S_L) is monotonically increased, which is attributed to the substantial enlargement in flame surface area (A_T/A_L). In contrast, the stretching factor (I_0) is almost constant and is smaller than 1, indicating a suppression effect of differential diffusion. By conducting the local flame dynamics analysis, the underlying mechanisms for these variations were revealed. On one hand, the local flame displacement speed S_d shows a strong negative correlation with flame curvature while such negative correlation and the PDF of flame curvature are only weakly influenced by u'/S_L. This explains the almost constant I_0 across different turbulence intensities. On the other hand, the PDF of the tangential strain rate is found to span a much wider range and shift to the positive side as u'/S_L increases, suggesting that the enhanced tangential strain rate is the main cause of the increase in the surface area (A_T/A_L) of turbulent premixed cool flames.

Third, the influence of equivalence ratio on above observations was demonstrated to be insignificant. This indicates that although the local reactivity of turbulent premixed cool flame is subjected to considerable differential diffusion effects, the resultant turbulence-flame-stretch interaction is insensitive to the equivalence ratio.

Throughout the analysis, the turbulent premixed cool flame is shown to feature some similar characteristics as the turbulent hot flames with Lewis number larger than 1, such as the strong negative correlation between the local flame displacement speed and flame curvature and the suppression effect of differential diffusion on the global flame speed, but more importantly, it also presents some unique characteristics which are distinct from hot flames, such as the weak sensitivity of flame structure to turbulence intensity and the weak sensitivity of flame dynamics to equivalence ratio. In this context, it is believed that this study can help gain better understanding about the

turbulent premixed cool flames. Nevertheless, it should be also noted that only one temperature and pressure condition was considered in this study, and thus it merits further investigation on the turbulent cool flame dynamics at a wider range of temperatures and pressures.

CRediT authorship contribution statement

Yiqing Wang: Writing – original draft, Methodology, Formal analysis, Conceptualization. **Chao Xu:** Writing – review & editing, Supervision, Conceptualization. **Cheng Chi:** Writing – review & editing, Software. **Zheng Chen:** Writing – review & editing, Supervision, Funding acquisition.

Declaration of competing interest

The authors declare that they have no known competing financial interests or personal relationships that could have appeared to influence the work reported in this paper.

Acknowledgments

This work was funded by NSFC, China (No. 52425604). The work at Argonne National Laboratory was supported by the U.S. Department of Energy, Office Of Energy Efficiency and Renewable Energy, under contract DE-AC02-06CH11357. C. Chi would like to thank the Deutsche Forschungsgemeinschaft (DFG), Germany for its support within Project TH881/38-1 (DADOREN).

Appendix A. Supplementary data

Supplementary material related to this article can be found online at https://doi.org/10.1016/j.combustflame.2024.113759.

References

[1] Y. Ju, Understanding cool flames and warm flames, Proc. Combust. Inst. 38 (1) (2021) 83–119.
[2] S.A. Skeen, J. Manin, L.M. Pickett, Simultaneous formaldehyde PLIF and high-speed schlieren imaging for ignition visualization in high-pressure spray flames, Proc. Combust. Inst. 35 (3) (2015) 3167–3174.
[3] A. Krisman, E.R. Hawkes, M. Talei, A. Bhagatwala, J.H. Chen, A direct numerical simulation of cool-flame affected autoignition in diesel engine-relevant conditions, Proc. Combust. Inst. 36 (3) (2017) 3567–3575.
[4] G. Borghesi, A. Krisman, T. Lu, J.H. Chen, Direct numerical simulation of a temporally evolving air/n-dodecane jet at low-temperature diesel-relevant conditions, Combust. Flame 195 (2018) 183–202.
[5] C.B. Reuter, S.H. Won, Y. Ju, Experimental study of the dynamics and structure of self-sustaining premixed cool flames using a counterflow burner, Combust. Flame 166 (2016) 125–132.
[6] S. Deng, D. Han, C.K. Law, Ignition and extinction of strained nonpremixed cool flames at elevated pressures, Combust. Flame 176 (2017) 143–150.
[7] M. Hajilou, M.Q. Brown, M.C. Brown, E. Belmont, Investigation of the structure and propagation speeds of n-heptane cool flames, Combust. Flame 208 (2019) 99–109.
[8] M.Q. Brown, E.L. Belmont, Effects of ozone on n-heptane low temperature chemistry and premixed cool flames, Combust. Flame 225 (2021) 20–30.
[9] Q. Yang, P. Zhao, Minimum ignition energy and propagation dynamics of laminar premixed cool flames, Proc. Combust. Inst. 38 (2) (2021) 2315–2322.
[10] Y. Wang, W. Han, T. Zirwes, F. Zhang, H. Bockhorn, Z. Chen, Effects of low-temperature chemical reactions on ignition kernel development and flame propagation in a DME-air mixing layer, Proc. Combust. Inst. 39 (2) (2023) 1515–1524.
[11] Y. Wang, W. Han, Z. Chen, Effects of stratification on premixed cool flame propagation and modeling, Combust. Flame 229 (2021) 111394.
[12] A. Krisman, E.R. Hawkes, J.H. Chen, Two-stage autoignition and edge flames in a high pressure turbulent jet, J. Fluid Mech. 824 (2017) 5–41.
[13] A.G. Novoselov, C.B. Reuter, O.R. Yehia, S.H. Won, M.K. Fu, K. Kokmanian, M. Hultmark, Y. Ju, M.E. Mueller, Turbulent nonpremixed cool flames: Experimental measurements, direct numerical simulation, and manifold-based combustion modeling, Combust. Flame 209 (2019) 144–154.
[14] A.G. Novoselov, C.K. Law, M.E. Mueller, Direct numerical simulation of turbulent nonpremixed "cool" flames: Applicability of flamelet models, Proc. Combust. Inst. 37 (2) (2019) 2143–2150.
[15] S. Farjam, B. Savard, Ignition and flame stabilization of n-dodecane turbulent premixed flames under Spray A thermochemical conditions, Combust. Flame 242 (2022) 112133.
[16] B. Savard, H. Wang, A. Teodorczyk, E.R. Hawkes, Low-temperature chemistry in n-heptane/air premixed turbulent flames, Combust. Flame 196 (2018) 71–84.
[17] D. Goodwin, H. Moffat, R. Speth, Cantera, 2015, http://www.cantera.org.
[18] B. Bobbitt, S. Lapointe, G. Blanquart, Vorticity transformation in high Karlovitz number premixed flames, Phys. Fluids 28 (1) (2016) 015101.
[19] S. Lapointe, B. Savard, G. Blanquart, Differential diffusion effects, distributed burning, and local extinctions in high Karlovitz premixed flames, Combust. Flame 162 (9) (2015) 3341–3355.
[20] S.H. Kim, Leading points and heat release effects in turbulent premixed flames, Proc. Combust. Inst. 36 (2) (2017).
[21] J. Bell, M. Day, J. Grcar, M. Lijewski, Active control for statistically stationary turbulent premixed flame simulations, Commun. Appl. Math. Comput. Sci. 1 (1) (2007) 29–51.
[22] A. Abdelsamie, G. Fru, T. Oster, F. Dietzsch, G. Janiga, D. Thévenin, Towards direct numerical simulations of low-mach number turbulent reacting and two-phase flows using immersed boundaries, Comput. & Fluids 131 (2016) 123–141.
[23] S. Lapointe, K. Zhang, M. McNenly, Reduced chemical model for low and high-temperature oxidation of fuel blends relevant to internal combustion engines, Proc. Combust. Inst. 37 (1) (2019) 789–796.
[24] T. Ombrello, S.H. Won, Y. Ju, S. Williams, Flame propagation enhancement by plasma excitation of oxygen. Part I: Effects of O3, Combust. Flame 157 (10) (2010) 1906–1915.
[25] N. Peters, Turbulent combustion, Meas. Sci. Technol. 12 (11) (2001) 2022.